POSITION SYNCHRONIZATION OF AEROSPACE ELECTROMECHANICAL ACTUATORS FOR DISTRIBUTED ELECTRICAL ACTUATION SYSTEM

Jian FU*, Jean-Charles MARE, Yongling FU***
***Beihang University, 100191 Beijing, China**
**** Institut Clément Ader, INSA-Toulouse, 31077 Toulouse Cedex 4, France**

Abstract

In the field of more electric aircraft, electromechanical actuators (EMAs) are becoming more and more attractive because of their outstanding benefits of aircraft fuel reduction, maintenance costs saving, and system flexibility improvement. For aerospace electromechanical actuator applications, the proposed communication addresses the combination of extensive use of EMAs and electrical synchronization. Two EMAs drive two independent loads which positions are to be synchronized at any time. Due to the different natural dynamics and loads, the two independent driven loads tend to get a different position, which is not acceptable. Even in case one actuator failure, priority is given to synchronization instead of following the position setpoint. Therefore, virtual prototype of the EMAs actuation system is proposed to assess and pre-validate the synchronization concepts with resort to a model-based approach.

1 Introduction

As the rapid growth of air traffic market in recent years, man-made CO_2 emissions into the atmosphere increased largely by civil aviation. The aircraft industry has to face both economic and environmental issues. In recent years, “More Electric” and “All Electric” aircraft concepts are becoming widely interested in aerospace industry for extended developing greener technologies for the next generation air transport.[1] Based on these concepts, the use of electrical power is increasing to replace the well-established hydraulic, pneumatic and mechanical power networks. Due to the mature power-by-wire (PbW) techniques,[2] two series of PbW actuators, electro-hydrostatic actuator (EHA) and electro-mechanical actuator (EMA) have been developed, which there may be architectural changes, for example electric-backup hydraulic actuator (EBHA) and electric-backup mechanical actuator (EBMA). These PbW actuators have already entered into service in the latest commercial aircraft programs. In Airbus A380/A350, EHAs are served as backup actuator for primary flight control and EBHAs are applied for spoilers control. In Boeing B787, EMAs are partly put on the front line for secondary flight control and landing gear braking. And in Airbus A400M, EBMA is applied as the function of open/close the main landing gear doors. Compared to EHA, EMA now is becoming more and more attractive because of its full elimination of the conventional local or centralized hydraulic circuits, which brings outstanding benefits of aircraft fuel reduction, maintenance costs saving, and system flexibility improvement.[3]

The safety issues are very demanding for the design and operation of commercial aircrafts. When EMA comes to perform critical functions, such as primary flight controls, the reliability aspects become more preponderant. Therefore, the different redundant configurations in aircraft impact the design objectives to reduce the probability of “loss of control” of the driven surface. In some applications, the surface itself is split into two parts and the actuation system has redundant power paths to drive the surface for performing position control: thrust reverser actuation system (e.g. TRAS), secondary flight controls (e.g. flap/slat) and pylon conversion of tilt-rotors (e.g. AW609). For the time being, all of these actuation systems use the same concept to ensure synchronization in a reliable way: the

loads are mechanically linked with interconnecting shafts (e.g. flexshafts for thrust reverse). Therefore, new features could be offered by managing independently the loads positions. In this attempt, the mechanical linkages between loads could be removed and position synchronization could be performed by mean of electrically signaled synchronization loops. This particularly concerns secondary flight controls. On the first hand, this could increase performance, facilitate integration within the airframe and even improve safety through multiple redundancies. On the second hand, large commercial aircraft could take advantage of "electrical synchronization" by using multiple secondary flight control actuators instead of centralized power control units (PCU) in order to balance the huge airload and to meet the installation space constraints.[4]

The proposed communication addresses the combination of extensive use of EMAs and electrical synchronization. In the proposed study, two EMAs drive two independent loads which positions are to be synchronized at any time. This is e.g. representative of thrust reverse or pylon conversion applications. Due to the different natural dynamics and loads, the two independent driven loads tend to get a different position, which is not acceptable. Therefore, the synchronization of the surfaces is realized by mean of control under the constraint of keeping a high level of segregation between the two actuation channels. In case one actuator failure, priority is given to synchronization instead of following the position setpoint.

2 Actuators and Redundancy Architectures

2.1 Types of actuator

In civil aircraft, the flight control actuators are servo controlled and are used to position a flight control surface to follow a setpoint. The conventional actuator is hydraulic servo actuator (HAS), which is fully hydraulic supplied by an centralized hydraulic network. Nowadays, with the development of “More Electric Aircraft”, more electrically powered actuators have been employed, such as EHA, EBHA, and EMA. As shown in Fig.1, the structure and relation of actuators are detailed presented.

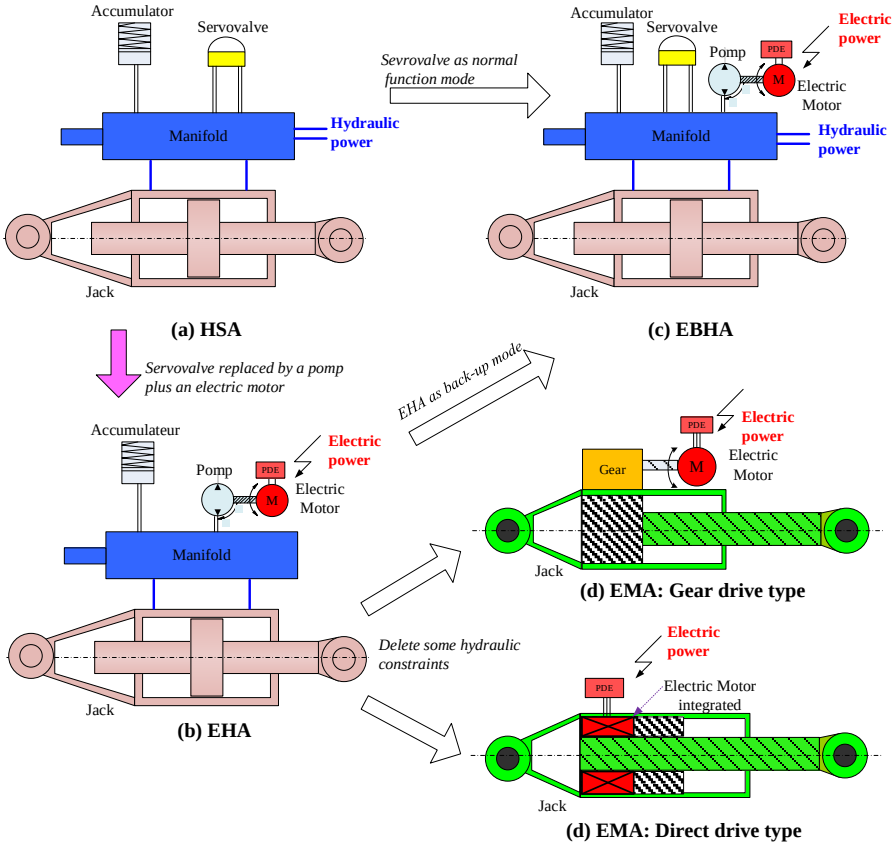

Fig. 1. Structure of common flight controls actuators

2.2 EMA redundancy architectures

EMA is considered as the ultimate concept of powered electrically actuator for future All/Full Electric Aircraft application, and right now it takes the most popular research interests. However, considered the safety issues and reliability requirements for EMA implementation, especially the critical actuation systems of the aircraft have to be redundant.[5] The common configurations of dual redundancy is summarized in Fig.2.

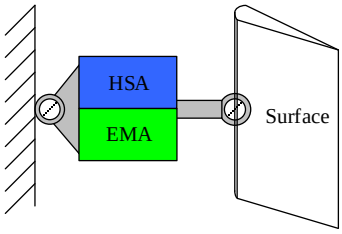

(a) Internal redundancy

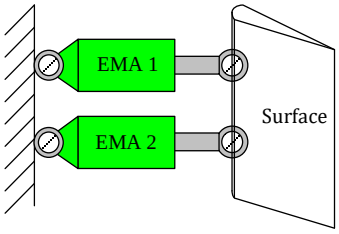

(b) Actuator redundancy

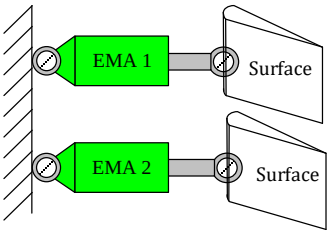

(c) Surface redundancy

Fig.2. Redundant EMA configurations

For internal redundancy configuration of Fig. 2(a), a cylinder integrates two power paths of hydraulic and electric to drive a single actuator arm. However, this configuration unable to completely avoid the presence of common failure points and just tolerates a failure in the power path, a complex jamming-free mechanism should be designed for grantee the security.

Fig.2(b) shows the most common solution for redundancy design. A single moving surface is driven by two EMAs, they could operate in active/standby mode, only one EMA is in charge of the positioning function while the other operates as a damper. The roles are reversed in case of the failure of the active channel. While EMAs work in active/active mode, they should equally drive the load, so “force fighting”[6] problem between two channels should be solved, which may bring additional force/torque and energy consumption. These two cases are both based on the EMA can be jamming-free, however the mechanism design is not easy and with high reliability when applied for primary flight controls.

Fig.2(c) provides a more attractive solution to reduce the probability of “loss of control” of the load. In aircraft, assumed the huge surface can be split into multiple small surfaces, they availably perform a same control mission. Such as the function of spoilers and slats, they are used for reducing lift as well as increasing drag, each surface has a small size, so they can be driven by a single EMA. In case of failure, the EMA can be locked in failed position, works on damping or free mode, or return to a defined position. And the remaining surfaces are operating in normal mode.

2.3 Position synchronization

Position synchronization can be found in very early aircraft and today’s industry process control system, it is performed by hydraulically, using flow dividers or by dedicated strategies that elaborate the control signal of each servo-valve. In nowadays aircraft, position synchronization is mostly achieved by mechanically, such as TRAS control. Although the mechanical position synchronization is mature, the potential failure of mechanical shaft (jamming) may cause the entire flap or slat of high lift system to loss of control. And mechanically synchronization is not very flexible and requires additional installation space.

This paper shows a concept of electrically position synchronization, two loads individually driven by two EMAs, as shown in Fig.3. The control law for position synchronization of the two loads is implemented in the control electronic units that pilot the power drive electronics (PDE) associated with each motor of EMA. The electronic control units (or actuator control electronics, ACE) of the actuators can also exchange data between each other via an

electrical connection. The control units are in charge of generating the movement sequence of the two loads, to regulate the position and to synchronize the load's position in any case. This electrically solution is more flexible and facilitates the realization of the position synchronization function.

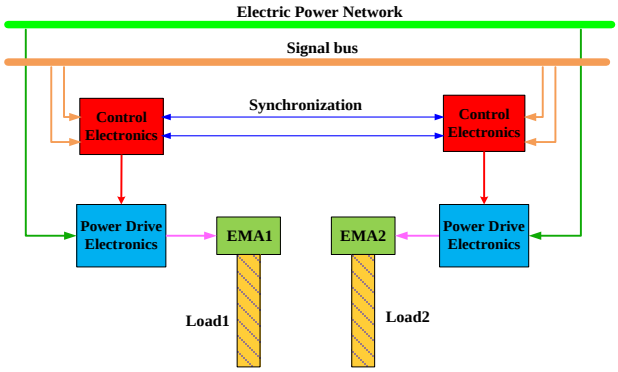

Fig.3. Electrically position synchronization of two independent EMAs

In future more electric aircraft, this concept of electrically synchronization of EMAs could be applied for electrical TRAS or developed in the field of secondary flight control actuation system by introducing a concept of "distributed actuation system", each surface of flap/slat driven by an independent EMA. In this paper, the structure of the studied actuation system is shown in Fig. 4: two EMAs drive two independent loads respectively, each actuator is controlled uniformly, locally and individually. The position synchronization control law is added in parallel between the two controllers.

3 Individual EMA Modeling

As shown in Fig.4, the studied EMAs system, each EMA is position servo controlled, it follows the position command and rejects the disturbance that is generated by the air load. The cascade control structure is applied: the inner loop of current in PDE, the middle loop of velocity and the outer loop of position in controller. Additional force sensor can be inserted between the EMA rod and the flight control surface in order to meet the rejection performance requirements through and additional force feedback. Monitoring information are collected by EMA controller, it is also in charge of running the Health and Usage Monitoring (HUM) algorithms and reporting the EMA faults to the top level flight control computers (FCCs).[7]

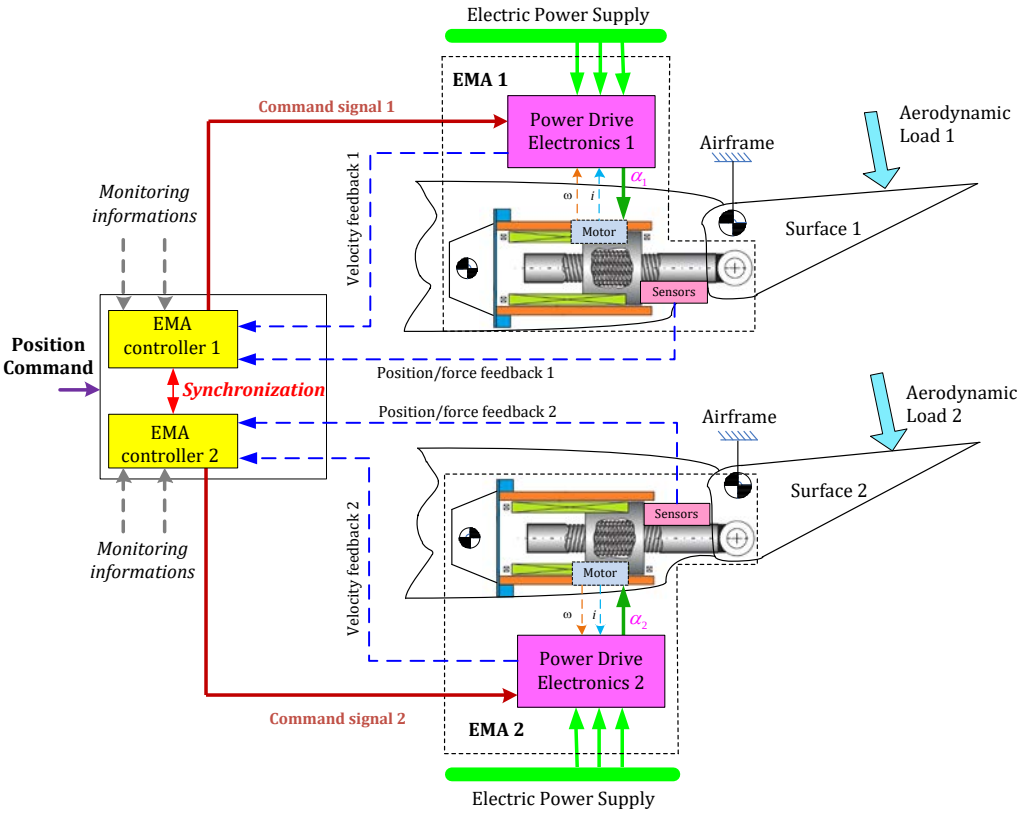

Fig.4. System studied of electrically position synchronization of two independent EMAs

3.1 Linear model of single EMA

A single direct drive EMA consists of five parts: (1) PDE which meters the power delivered to motor from electric power supply; (2) EM which transforms the electrical power to mechanical; (3) Screw nut mechanism which transforms mechanical power between the high speed/low torque rotational and the low velocity/high force translational for the load; (4) sensors of current, velocity, position and force. (5) ACE which performs closed loop control. The load (flight control surface), not part of the EMA model, is simply modelled as an equivalent translating mass to which the air load is applied. For controller design, the basic model of EMA is selected[8], some complex nonlinearities in these components can be neglected, such as friction (load, temperature effects), backlash/preload, magnetic saturation and the signal effects and etc.

3.2.1 PDE mathematic model

PDE is a four-quadrant three-phase inverter, it can be considered as a perfect modulated power transformer, for the preliminary design of controllers, it may be advantageous to develop a simplified model that merges the PDE and the motor, thus the dynamics of the current loop can be modelled as an equivalent second order model. And the relation of electromagnetic torque C_r (Nm) and motor referenced torque C^* (Nm) can be descripted as:

$$C_r = \frac{\omega_i^2}{s^2 + 2\xi_i\omega_i s + \omega_i^2} C^* \tag{1}$$

where s is the Laplace variable, the two parameters $\omega_i = 2\pi f_i$ and ξ_i are the current (torque) loop natural frequency (rad/s) and the dimensionless damping factor, respectively. These parameters can be provided by the PDE supplier (typically f_i is in the range 600-800 Hz while ξ_i is in the range 0.6 to 1).

3.2.2 Electric motor mathematic model

The electric motor is most of the 3-pahse type, BLDC or PMSM. For basic model, the motor can be seen as a perfect power transformer in which the torque balance:

$$C_m = K_m I_m - J_m \frac{d\omega_m}{dt} \tag{2}$$

where C_m is the motor output torque (Nm), K_m is the motor electromagnetic constant (Nm/A), J_m is the rotor inertia (kgm^2), ω_m is motor velocity (rad/s).

3.2.3 Screw nut mechanism mathematic model

The basic model of screw nut can be considered as perfect, it achieves pure power transformation between the electric motor and the load with a ratio ($2\pi/p$):

$$\begin{cases} F_L = 2\pi C_m / p \\ V_L = p\omega_m / 2\pi \end{cases} \tag{3}$$

where p is the pitch (m) of screw nut mechanism, F_L and V_L are respectively the force (N) and velocity (m/s) from EMA to drive the load.

3.2.4 Compliance or stiffness consideration

For EMA control design, most analysis and research work uses a linear first or at most second order system to represent the EMA. Thus, the inner compliance (i.e. screw nut) and outer compliances (the anchorage to airframe and the transmission to load) are all neglected. However, the compliances have a big effect on EMA dynamic performance. Thus, the main sources of compliance are introduced by adding the anchorage k_a (N/m) and transmission k_t (N/m) stiffness coming from the aircraft structure and the global stiffness of the EMA internal mechanical transmission k_n (N/m) that merge the contributions of the nut-screw, the bearing and joints. To simplify the study, structural compliances at the anchorage of the EMA housing to the airframe and at the EMA rod to load connection are merged into a single stiffness k_s (N/m) model that is inserted in series between the rod and the load, expressed as:

$$k_s = \frac{k_a k_t}{k_a + k_t} \tag{4}$$

In these conditions the inertia effect of the rod mass of cylinder M_t (kg) should be taken into account. The motor equivalent mass M_m (kg) and motor equivalent output force can be calculated as:

$$M_m = \frac{4\pi^2}{p^2} J_m, \quad F_m = \frac{2\pi}{p} C_m \tag{5}$$

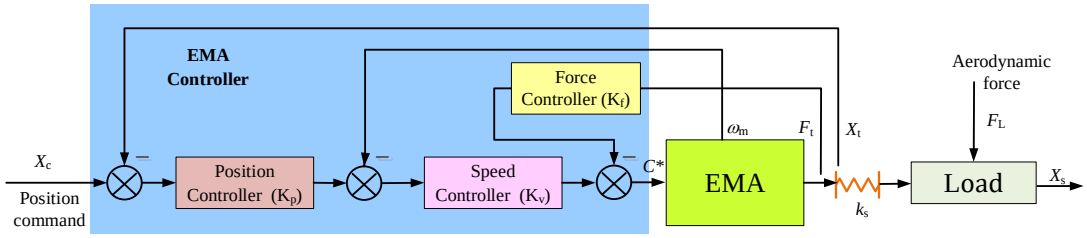

Fig.5. Controller structure of independent EMA

3.2.5 Controller structure

The control structure of the EMA is shown in Fig.5. The EMA controller implements the cascade common structure. K_p, K_v and K_f are the propositional gain of position, velocity and force feedback controller. Two saturation functions are generally inserted to limit the speed and the torque demands. respectively. The current controller is integrated in the PDE model of EMA. Position command is X_c (m), feedback is rod displacement X_t (m), and the load displacement is X_s (m). Disturbance force from the aerodynamic is F_L (N). Measured rod force for feedback control is F_s (N).

In Fig.5, the torque open-loop model of the EMA has two inputs of torque demand C^* and aerodynamic force F_L, one output of the rod displacement X_t.. Using state space method to get the EMA open loop model, the input vector of EMA is $\mathrm{U}=[C^* \quad F_L]^T$, the output variable is $y=X_t$. The state vector is $\mathrm{X}=[\omega_m \quad F_m \quad \dot{X}_t \quad F_t \quad \dot{X}_s \quad X_t]^T$. The state space model using Laplace transformation is:

$$\begin{cases} sX_t(s)=\boldsymbol{A}X_t(s)+\boldsymbol{B}U(s) \\ Y(s)=\boldsymbol{C}X_t(s)+\boldsymbol{D}U(s) \end{cases} \tag{6}$$

where,

$$\boldsymbol{A}=\begin{bmatrix} 0 & -\frac{2\pi}{pM_m} & 0 & 0 & 0 & 0 \\ \frac{pk_n}{2\pi} & 0 & -k_n & 0 & 0 & 0 \\ 0 & \frac{1}{M_t} & 0 & -\frac{1}{M_t} & 0 & 0 \\ 0 & 0 & k_s & 0 & -k_s & 0 \\ 0 & 0 & 0 & \frac{1}{M_s} & 0 & 0 \\ 0 & 0 & 1 & 0 & 0 & 0 \end{bmatrix} \tag{7}$$

$$\boldsymbol{B}=\begin{pmatrix} \frac{16\pi^4}{p^4M_m} & 0 & 0 & 0 & 0 & 0 \\ 0 & 0 & 0 & 0 & \frac{1}{M_s} & 0 \end{pmatrix}^T \tag{8}$$

$$\boldsymbol{C}=\begin{pmatrix} 0 & 0 & 0 & 0 & 0 & 1 \end{pmatrix} \tag{9}$$

$$\boldsymbol{D}=\begin{pmatrix} 0 & 0 \end{pmatrix} \tag{10}$$

Consequently, the output X_t can be expressed by

$$X_t(s)=\boldsymbol{C}(s\boldsymbol{I}-\boldsymbol{A})^{-1}\boldsymbol{B}\boldsymbol{U} \tag{11}$$

where $\boldsymbol{I}$ is unitary matrix.

According to the above equations, the open loop transfer of rod displacement in response to torque demand C^* and load disturbance F_{ex} is of 6th order. In practice, the rod mass (a few kg) is very small when compared to the equivalent motor mass (rotor reflects at the load level) through the mechanical transmission, see eq.(5). For this reason, the 6th order can be reduced to 4th order for preliminary controller design.

3.2 Full model of single EMA

In realistic, EMA has the multidisciplinary effect, include electrical, magnetic, mechanical, and thermal. Electrical effect are: the conduction loss and switching loss of semiconductor in PDE, and copper loss in motor. The magnetic effect mainly is iron loss and saturation in motor. Mechanical effect are cogging torque in motor, friction loss and backlash/preload in screw nut mechanism. The losses cause the heat, and make the temperature increased of EMA surrounding, temperature increased that makes more losses, this may cause a snowball effect. In addition, temperature affect the dynamic performance, service life, and reliability of EMA components. Thus, for full EMA model the thermal effect of

power losses should be considered. In our previous work [8], Multi-level EMA models have been presented, in the following study, the advanced models are considered.

4 Strategy of Position Synchronization

4.1 Control goal

According to the above configuration of EMAs system of Fig.4, each channel is independent and available for two EMAs position synchronization. The control goal is to achieve satisfactory reduction of the position difference between the two independent loads, shown in Fig.6.

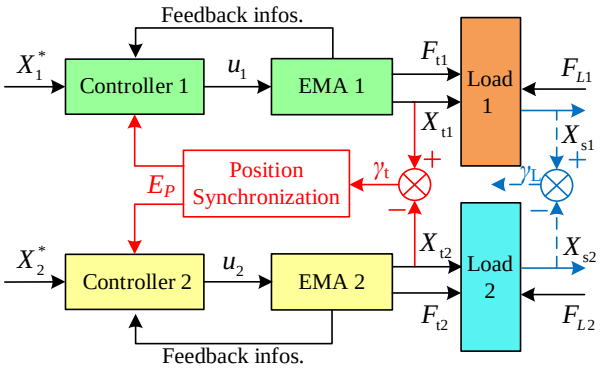

Fig.6. Architecture of position synchronization

In theory, the position two loads should be always identical with the position command (setpoint) X_c of pilot or autopilot at any time:

$$X_{s1} = X_{s2} = X_c \quad , \quad \forall F_{L1}, F_{L2} \tag{12}$$

In addition, EMAs applied for aerospace critical application should have the fault tolerant. It means that in the case of one EMA fails, the other should not to follow the position setpoint X_c but to achieved the same position as the failed one. Thus two independent EMAs must keep their position synchronized strictly:

$$X_{s1} = X_{s2} \quad , \quad \forall X_{s1}, X_{s2} \neq X_c \tag{13}$$

The position synchronization strategy is to eliminate or reduce the synchronization error between the two loads γ_L:

$$\gamma_L = X_{s1} - X_{s2} \tag{14}$$

However, in aircraft actuation system, the load position cannot be measured directly for servo control, so the desired γ_L is difficult to be acquired. The position can be measured is the road extension of EMA, using LVDT, so the position synchronization error γ_t of EMAs can be defined as:

$$\gamma_t = X_{t1} - X_{t2} \tag{15}$$

4.2 Strategy structure

Concerning the position synchronization, most of the research works are related to synchronized motion control of multi-axis machine tools, and the master-slave synchronization structure is applied.[9,10] Thus, one machine EMA (slaved) is position controlled to follow the position of the other (master one). This master-slave solution may applied for EMAs, however when the slave channel is failed, the system can't normally work. Moreover, the slave load is always delayed in comparison with the master load due to the dynamics and servo lag of the slave channel. Thus, the additional control compensation should be added, that may increase the complexity of the controller.

Another position synchronization method is using cross coupled synchronization (CCS) structure, which is widely implemented in industry. The advantage is that the servo lag delay can be eliminated. The control structure can be strictly identical for each channel. Two EMAs receive the same position command simultaneously. Each one is closed-loop position controlled independently with additional position synchronization inputs.

$$X_1^* = X_2^* = X_c \tag{16}$$

4.3 CCS Controller Design

The requirements for the CCS controller design are listed below:

- The position synchronization controller shall eliminate (ideally), or as far as possible reduce synchronization error (γ_L) to an acceptable level in any case of normal operation;
- When one channel failed, the other must be controlled at the same position as that failed one. Therefore, it is accepted that

the loads' positions cease to follow the position setpoint;

- The closed loop performance (pursuit and rejection) of each EMA shall not be significantly influenced by the position synchronization.

At each EMA local level, position synchronization is implemented introducing a synchronization input. This input is calculated as a function of the sensors signals that are already available for the position control of each EMA (EMA extension, motor speed/position, transmitted force to load). The simplest and most direct approach of design CCS consists in elaborating the position synchronization signal as a dynamic function of the EMAs extensions difference (γ_t). This signal is injected as an additional torque demand (C_s) into each EMA torque reference (C^*).

Two options can be applied for CCS controller, first one is hybrid structure that can introduce the velocity signals directly. Using the motor speed signals that are used for implementation of the field oriented control (FOD). The other is also possible to introduce the velocity signals but as the differential signals from rod position through the D action of PID controller. The two candidate CCS structures are shown in Fig. 7 (a) and (b).

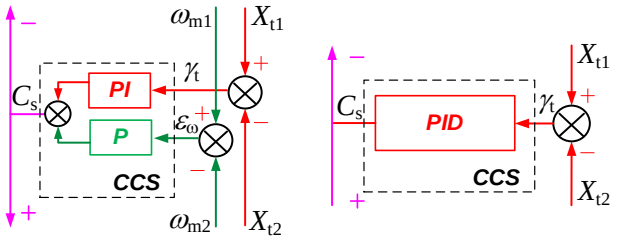

(a) Hybrid CCS (b) Single PID-CCS

Fig.7. Two types of CCS controller

Fig.7 (a) displays the CCS structure that uses both position error (γ_t) and motor velocity error (ε_ω) as input. The γ_t is controlled by a proportion-integral (PI) structure and ε_ω is introduced by a pure proportional action of gain P. Fig.7(b) simply uses the EMA extension signals and introduces the velocity difference through the PID action. In the same manner, the derivative effect D can be seen as an "electrical" equivalent of a damper connecting the two EMAs rods.

Comparing this two structures, because of the parasitic effect of compliance/backlash in screw nut mechanism of EMA, the rod velocity and motor velocity not simply proportional. If a failure of free-play occurs in screw nut mechanism, the motor speed is not null but the rod speed is null, that will cause the big error and controller is failure. So the PID-CCS structure is more suitable for EMAs position synchronization when considered the important and common nonlinear effects.

In addition, when implementing PID-CCS structure, for safety reason it should to limit cross-coupling effects between the two channels. A saturation element can be added after synchronization PID function. As well, the low-pass filtering of the derivative action and anti-windup of the integral action are also need to be considered for stability.

The total control structure of two EMAs for position synchronization according to the PID-CCS position synchronization is shown in Fig. 8. The individual EMA controller, the multi-feedback controller (position/speed/force) has been studied and presented in section 3.2.5. The CCS controller between the two EMAs is clearly evident, by noting the interconnections of synchronization position tracking error of γ_t. The synchronization torque demand (C_s) is summed to the torque demand coming from the individual EMA controller.

The proposed two criterions are defined in order to quantify the performance of the load position synchronization by using PID-CCS structure. They are calculated as:

(1) E_{ITAE} as the integral of time-weighted absolute error (ITAE):

$$E_{ITAE} = \int_0^\infty t\left|\gamma_s(t)\right| dt \qquad (17)$$

(2) E_{max} as the absolute maximum value of position synchronization error:

$$E_{MAX} = MAX\left\{\left|\gamma_s(t)\right|\right\} \qquad (18)$$

where t is the time.

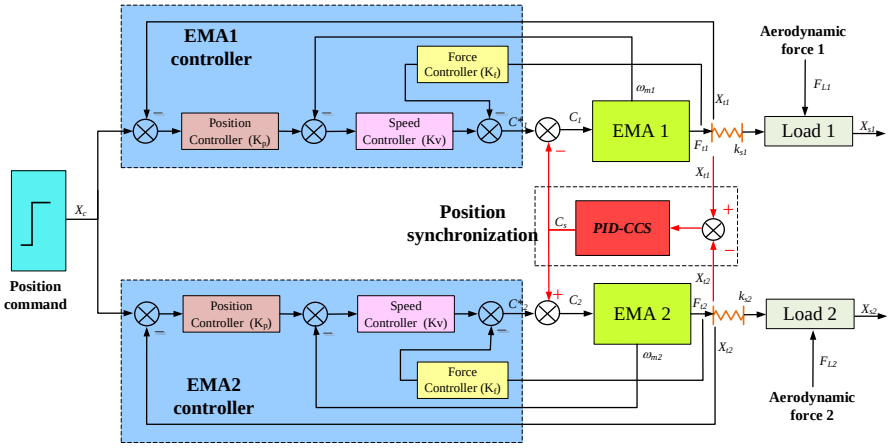

Fig.8. Schematic of global structure of EMAs position synchronization

5 Virtual Prototype of Synchronized EMAs

5.1 Linear virtual prototype

As a first step, a linear approach is used to formally define the structure and to support the parameter setting of the position synchronization function added to the individual position control. The performance, either in frequency or in time domain, can be assessed without numerical simulation through the theory of linear systems. It is interesting to also implement the linear model as simulation model to meet engineering need of the control design. In that manner, the influence of nonlinear effects can be easily assessed by replacing the linear model by the advanced model.

Fig.9 displays the linear model implemented for simulation in the MATLab/Simulink environment. All the parasitic effects of PDE dynamics, EM electrical and frictional effects, MPT inertial and frictional effects, and digital implementation of control (anti-aliasing, sampling, and quantization) are not considered. The compliance effects are taken into account as linear effect because of their impact on force rejection performance.

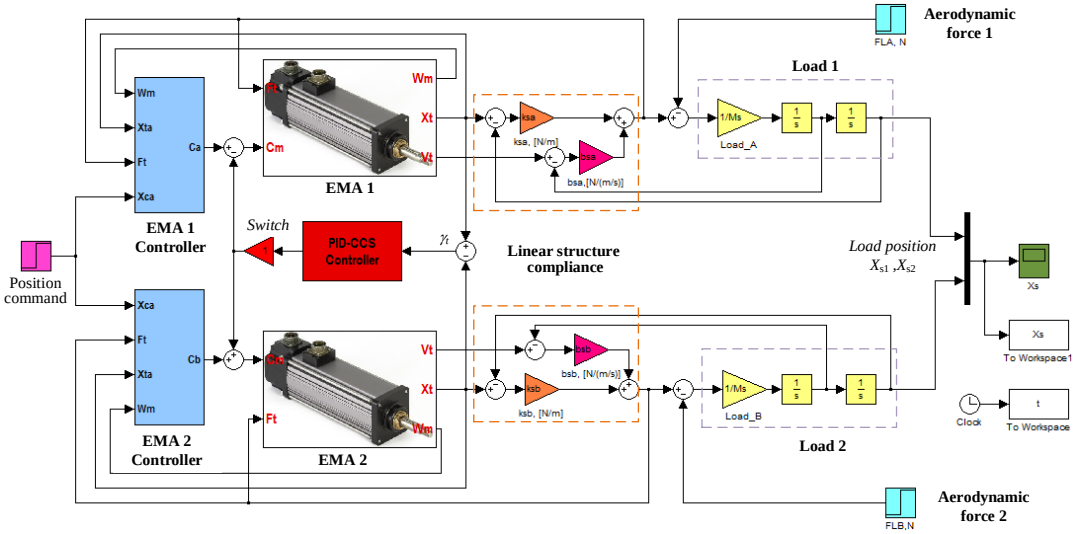

Fig.9. Linear virtual prototype for EMAs position synchronization in MATLab/Simulink

5.2 Full virtual prototype

All the former mentioned physical effects (nonlinearities) are considered in the full virtual prototyping model implemented in the LMS-AMESim simulation environment, as shown in Fig.10, including the proposed position synchronization control method. At the same time, other parasitic effects associated with the test and the instrumentation are also considered.

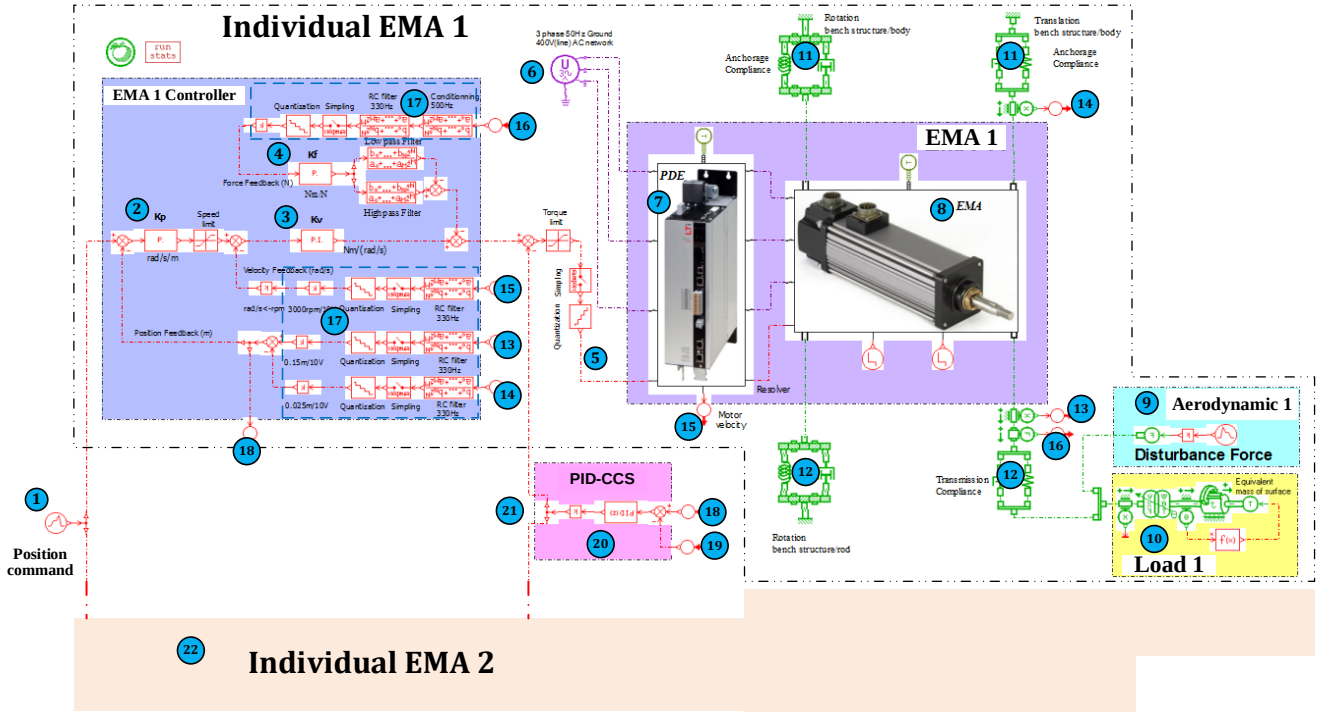

Fig.10. Full virtual prototype for EMAs position synchronization in LMS-AMESim

This full model consists of following components:

(1) Position command $X_{c.}$

(2) EMA 1 position feedback loop and proportional control gain.

(3) EMA 1 velocity feedback loop and proportional control gain.

(4) EMA 1 force feedback loop and proportional control gain.

(5) EMA 1 torque control reference.

(6) Electric power supply for EMA 1.

(7) Power drive electronics (PDE) advanced submodel of EMA 1.[8]

(8) EMA 1 cylinder 2-DoF submodel (EM and MPT including).[8]

(9) Dynamic loading for EMA 1 (here an ideal and piloted source of force).

(10) Realistic inertial load of EMA 1.

(11) 2-DoF anchorage between EMA 1 body and airframe.

(12) 2-DoF transmission compliance between EMA 1 rod and inertial load.

(13) EMA 1 rod displacement from the position sensor of LVDT.

(14) EMA 1 anchorage deformation form LVDT sensor.

(15) EMA 1 motor velocity form PDE resolver.

(16) EMA 1 output force to load, form force sensor.

(17) Sensor dynamics, ADC filter, sampling and quantization.

(18) Relative displacement between the EMA 1 rod and test airframe.

(19) Relative displacement between the EMA 2 rod and airframe.

(20) Position synchronization controller PID-CCS.

(21) Torque compensated out of PID-CCS controller.

(22) Individual EMA 2 system, with same structure of EMA 1.

The full model of Fig.10 is more realistic, it includes the digital control effects, which are neglected in the linear model: filtering, sampling, quantizing and conditioning. It is particularly important to consider them because they may significantly impact performance (phase lag and noise). Moreover, the measured quantities will the discrete ones. The parameters associated with these electrical signaling effects are summarized in Tab.1.

Table. 1. Electrical nonlinear effects

Items	Description	AMESim Submodels
Filtering	First order low-pass filter placed on any A/D converter input	First order lag : f_{rc}=330 Hz
Sampling	Sampling rate for control: 0.5ms (2 kHz)	Zero order hold: t_s=0.5ms
Quantization	Quantization of A/D converter device: 14 bits for ±10V full scale	Quantize: 0.001V
Conditioning	Second order low-pass filter for EMAs and HSAs force sensors conditioning	Second order lag: ω=500Hz, ξ=0.8

5.3 Simulation results and analysis

5.3.1 Controller parameters

Simulations are run to illustrate the capability of the proposed EMA modelling and CCS-PID controller to assess the preliminary analysis of position synchronization performance. Models parameters are form our previous studies [7, 8]. The key controller parameters are listed in former Tab. 2 for following mission excitations applied to linear model and full model.

Table.2. Parameters of system controllers

Item	Parameter	Value
EMA individual controller	Position proportional gain K_p (Nm/m)	$5\ 10^5$
	Velocity proportional gain K_v (Nm/(rad/s))	0.5
	Force controller pure gain K_f (Nm/N)	0.005
	Force controller low-pass filter gain K_{lp} (-)	0.06
	Force controller low-pass filter frequency f_{lp} (Hz)	3
	Force controller high-pass filter gain K_{hp} (-)	0.6
	Force controller high-pass filter frequency f_{hp} (Hz)	15
PID-CCS controller	Position proposition gain K_{pr} (Nm/m)	$1\ 10^5$
	Integral gain K_{ir} (Nm s/m)	$8\ 10^5$
	Differential gain K_{dr} (Nm /(m/s))	$5\ 10^3$
Digital application in full model	Sampling period (s)	$5\ 10^{-4}$
	Quantization voltage (V)	0.001
	Discrete PID-CCS output torque limitation (Nm)	±10

5.3.2 Response of position step command

A 10 mm position step signal at t = 0.1 s is used to verify the position synchronization performance in the normal mode. The aerodynamic force are different, two disturbing force are square waves of 0.6 s period, the magnitude for EMA 1 is 5 kN (applied at t = 0.6) and the magnitude for EMA 2 is 15 kN (with a 0.3 s phase delay and applied at t = 0.9 s). The mission profile is shown in following Fig.11 (a). Fig.11 (b) and (c) shows the simulation results of the linear model and full model, separately.

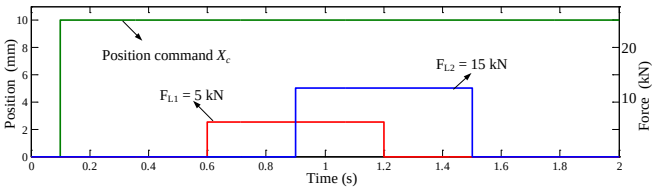

(a). Step mission profile

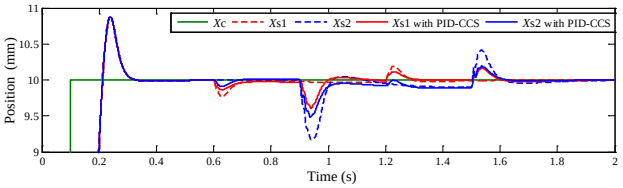

(b). Performance of linear model

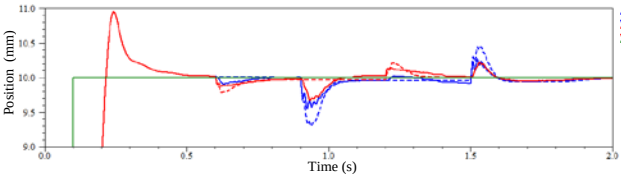

(b). Performance of full model

Fig.11. Performance of step command

From Fig. 11 (b) and (c), it can be noticed that the position synchronization controller (CCS-PID) has no effect on the pursuit performances (before t = 0.6 s). However, in both models, when different disturbance forces are applied (start at t = 0.6 s), the position difference clearly appear (the two dashed curves) and cannot be removed without resort to the CCS-PID controller. When introduced PID-CCS controller, the load position can be synchronized and the synchronization error is reduced. However, in the transient phase of the response, the mean value of the two actuators' position remains quite identical with and without the CCC-PID controller. The simulation results in full model show more oscillations and slower responses. This essentially comes from the more

realistic friction and compliance models and from the effect of digital implementation of the controllers.

Furthermore, comparisons of the absolute MAX and ITAE criterion performances for position synchronization error in linear model and full model, without/with PID-CCS synchronization controller could be calculated easily by using Eq.(16) and Eq.(17). By using PID-CCS controller, the maximum synchronization error between the two EMAs loads is reduced by 80% (from 0.81 mm to 0.17 mm) in linear model and by 58% in the full model.

5.3.3 Response of position trapezoidal command

A specific mission of trapezoidal position demand is created as between ± 50 mm with a slope of 50 mm/s that represents the maximum velocity input. Two different load disturbances are applied: for EMA 1, a step demand occurring at t = 0.5s with a magnitude of 10 kN. For EMA 2, a trapezoidal force signal that starting at t = 2s with a maximum magnitude of 10 kN, falling at t = 7s a static level of 2 kN. The mission profile is shown in Fig.12 (a). Fig.12 (b) and (c) are the interest of the comparison of synchronization errors for liner model and full model, separately.

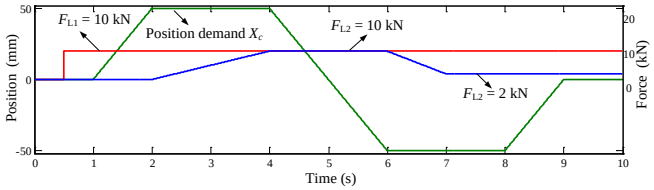

(a). Trapezoidal mission profile

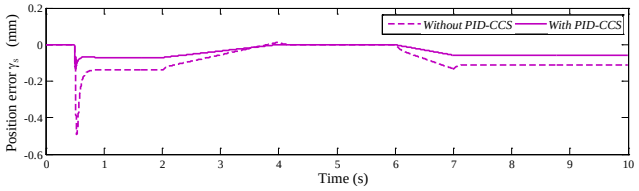

(b). Synchronization error of linear model

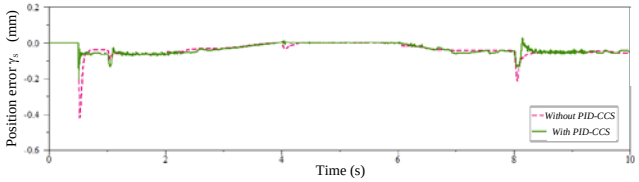

(c). Synchronization error of full model

Fig.12. Performance of trapezoidal command

As shown in Fig. 12 (b) and (c), with PID-CCS controller, the synchronization error is significantly reduced in both linear and full models. The full model simulation results show more high frequency/low magnitude oscillations that come from realistic structure compliance between EMA housing and frame., because the position feedback in full model presented the relative displacement of the EMA rod and the housing.

The evaluations of synchronization error for both the linear model and full model, also can be performed using the absolute MAX and ITAE criterion of Eq.(16) and Eq.(17), the results are listed in Tab. 3.

Table.3. Position synchronization error

Control Schema (PID-CCS controller)		Synchronization error γ_S (mm)	
		ITAE	MAX
Linear model	Without	3.8	0.49
	With	1.8	0.13
Full model	Without	1.9	0.43
	With	1.7	0.21

5.3.4 Response to failure

For response to failure of EMAs, jamming fault is considered, which is triggered on EMA 1. A specific mission consists of two position steps (30 mm from null at t = 0.1 s then -15mm from 30 mm at t = 3 s). The loads are of trapezoidal shape with different phase and level for each EMA. EMA 1 always operates normally while EMA 2 is jammed during its motion to reach the 30 mm position setpoint or when the loads change at t = 2 s. Fig.13 (a) shows the mission profile with two jamming triggering time, the aerodynamic is varied. Following this mission profile, Fig. 13 (b) and (c) show the position performance in the presence of jamming faults when the PID-CCS is active or not active for both linear and full models. Then, the position synchronization errors are plotted on Fig. 13 (d) and (f).

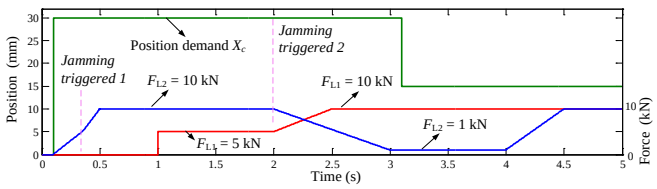

(a). Response to faults mission profile

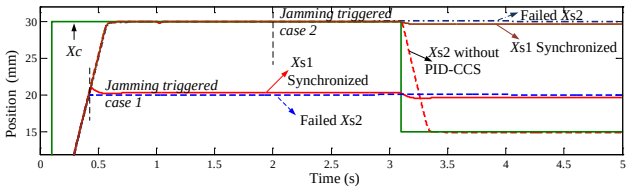

(b). Performance of linear model

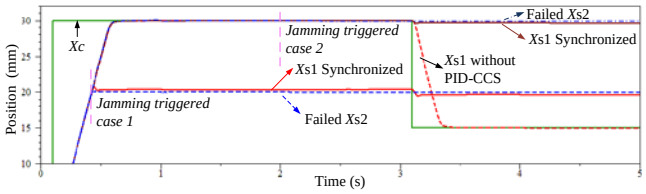

(c). Performance of full model

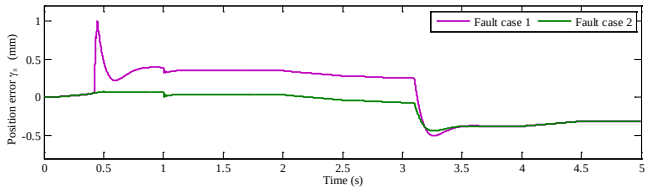

(d). Synchronization error of linear model

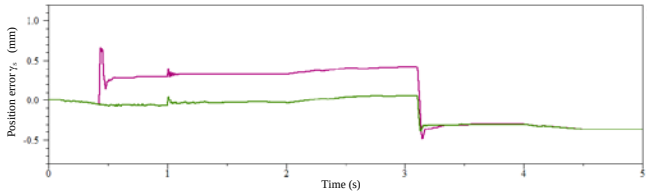

(e). Synchronization error of full model

Fig.13. Performance of response to fault

It can be seen form above results, position synchronization cannot be achieved without PID-CCS. Oppositely, the introduction of PID-CCS controller enables the healthy EMA to detect the fault and to synchronize to the faulty EMA, whatever the position demand. Although the position and synchronization controllers have been designed using the linear model, it is observed that they produced good results when applied to the full model. For the position synchronization performance of response to fault, it can be obtained that the loads position are well synchronized and with very small error. The maximum error ratio (E_{MAX}/Max travel) is 1.5% in linear model and 1.3% in full model when using proposed PID-CCS controller.

6 Conclusion

This communication addresses the combination of extensive use of EMAs and electrical synchronization. In the proposed study, for representation of thrust reverse or pylon conversion applications, two individual EMAs drive two independent loads which positions are to be synchronized at any time. The virtual prototype of the actuation system is proposed to assess and prevalidate the synchronization concepts with resort to a model-based approach. The position controller with synchronization feature is firstly designed on basis of a linear model of EMAs. Then a full model for realistic prevalidation is proposed with the consideration of more cross-linked physical effects and it can be adapted to the different engineering needs to make simulation as realistic as possible. Typical mission excitations are proposed to verify in a qualitative and quantitative way the synchronization performance. It is observed that the proposed PID-CCS controller is useful and can significantly reduce the position synchronization error at any time.

References

[1] Roboam X, Sareni B and Andrade A.D. More Electricity in the Air: Toward Optimized Electrical Networks Embedded in More-Electrical Aircraft. *IEEE Industrial Electronics Magazine*, December, pp.6-17, 2012.

[2] MARE J.-C, *Aerospace Actuator 1:Needs, Reliability and Hydraulic Power Solutuions*, 1st edition, Publisher, 2017.

[3] Mare J.-C, Fu, J. Review on signal-by-wire and power-by-wire actuation for more electric aircraft. *Chinese Journal of Aeronautics*, Vol.30, No.3, pp 857-871, 2017.

[4] Recksiek M. Advanced high lift system architecture with distributed electrical flap actuation. *Conference of Workshop on Aviation System Technology*, Hamburg, Germany, pp.1-11, 2009.

[5] Bennett J.W, Atkinson G.J, Mecrow B.C, and Atkinson D. J. Fault-tolerant design considerations and control strategies for aerospace drives. *IEEE Transactions on Industrial Electronics*, vol. 59, pp. 2049-2058, 2012.

[6] Arriola D and Thielecke F. Design of Fault-Tolerant Control Functions for a Primary Flight Control System with Electromechanical Actuators. *IEEE AUTOTESTCON*, National Harbor, pp. 393-402, 2015.

[7] Fu J, Mare J.-C, and Fu Y. Modelling and simulation of flight control electromechanical actuators with special focus on model architecting, multidisciplinary effects and power flows. *Chinese Journal of Aeronautics*, Vol.30, No.1, pp 47-65, 2017.

[8] Fu J, Mare J.-C, Yu L and Fu Y. Multi-level virtual prototyping of electromechanical actuation system for more electric aircraft. Chinese Journal of Aeronautics, Vol.31, No.5, pp 892-913, 2018.

[9] Richiedei D, Synchronous motion control of dual-cylinder electrohydraulic actuators through a non-time based scheme. *Journal of Control engineering and applied informatics*, Vol.14, No.4, pp. 80-89, 2012.

[10] Chen C, Liao P. Fuzzy controller design for positioning and synchronization of electrohydraulic system. *Second IEEE Conference on Industrial Electronics and Applications*, Harbin, China, pp.971-976, 2007.

Contact Author Email Address

Corresponding Author: fujianbuaa@126.com

Copyright Statement